Miniaturized Permeability Assay for CRISPR-Mediated Genome-Wide Screens

by

Claire Simonneau[1], Junning Yang[1], Xianguo Kong[1], Robert Kilker[1], Leonard Edelstein[1], Paolo Fortina[3], Eric Londin[4], and Arie Horowitz[1,2ℵ]

1 – Cardeza Center for Hematology Research, 2 – Department of Cancer Biology, 3 – Sidney Kimmel Cancer Center Genomics Laboratory, 4 – Computational Medicine Center, Sidney Kimmel Medical College, Thomas Jefferson University, Philadelphia, Pennsylvania, USA.

ℵ – Corresponding author

Running title: Miniaturized permeability assay

Summary

We developed a new permeability assay in which endothelial cells are grown to confluence on ~150 μm microcarriers; each microcarrier is measured as a separate sample, facilitating a sufficiently large number for the performance of human genome-wide CRISPR screens.

Address for correspondence: Arie Horowitz, Cardeza Center for Vascular Biology, Sidney Kimmel Medical College, Thomas Jefferson University, 1020 Locust Street, Philadelphia PA 19107, USA.

Email: arie.horowitz@jefferson.edu

November 15, 2018

ABSTRACT

The integrity of epithelial or endothelial cell monolayers that coat the lumen of numerous body systems is crucial for the normal vertebrate physiology. The integrity of their intercellular junctions is the key element of monolayer barrier function. The repertoires of genes and proteins that mediate these signals are far from complete. Recently-developed high-throughput genome-wide screens could be used in principle to map these pathways, but this powerful approach cannot be easily adapted to collective cell functions. To overcome this limitation, we invented a new permeability assay based on monolayers grown on ~150 μm microcarriers. Each microcarrier functions as a miniature assay of permeability (MAP). Here we validate the assay by showing that the expression of short guide RNAs (sgRNAs) targeting genes coding known thrombin signaling proteins block effectively thrombin-induced junction disassembly, that and that microcarriers coated by such cells can be separated from those that carry cells expressing non-targeting sgRNAs, and that the detection sensitivity of MAP to gene repression is higher filter-based permeability assay.

INTRODUCTION

One of the new opportunities afforded by the sequencing of the human (and of many other organisms) genome is the ability to run genome-wide reverse screens to identify genes that underlie diverse phenotypes. The repurposing of CRISPR/Cas9 for targeting either repressive or activating modules to genomic loci generated a more versatile and specific tool than RNAi and became the screen method of choice. In the few short years since this tool became available, it has already been applied to numerous ends, including cancer drug discovery (Shi et al., 2015a), analysis of unfolded protein response (Adamson et al., 2016), and the identification of cancer immunotherapy targets (Manguso et al., 2017). CRISPR/Cas9-mediated screens take advantage of the accurate targeting to genomic loci specified by the sgRNA sequence to target disabled Cas9 (dCas9) fused to an either inhibitory or activating protein. Transcriptional activation has been achieved by various combinations of a range of modules, including NF-κB trans-activating subunit p65 (Konermann et al., 2015), tetrameric VP16 transactivation domain (VP64), heat shock factor 1, the catalytic histone acetyltransferase core domain of the human E1A-associated protein p300, and the viral replication and transcription activator (Rta) [reviewed in (Chavez et al., 2016)]. In contrast, transcriptional repression has been produced by a single module, the Krüppel-associated box (KRAB) domain of the zinc-finger transcription factor Kox1(Gilbert et al., 2014; Kearns et al., 2014; Thakore et al., 2015). The efficacy of the regulatory dCas9-fused module is highly dependent on the selection of the genomic targets of the sgRNA relative to the transcription start sites based on rules that were derived and optimized empirically (Horlbeck et al., 2016; Konermann et al., 2015). Activation on the order of 10^3-fold, as measured by quantifying mRNA levels of selected genes, was achieved by some of the above complexes (Chavez et al., 2016), whereas transcriptional repression measured in the same way was on the order of 10^2-fold, and rarely 10^3-fold (Gilbert et al., 2014).

Genome-wide screens employing activating or repressive dCas9 constructs and sgRNA libraries were deployed to identify toxin or drug resistance and vulnerability conferring genes (Chen et al., 2015; Gayle et al., 2017; Gilbert et al., 2014; Kurata et al., 2016; Tao et al., 2016; Yamauchi et al., 2018), genes that mediate cell immune and inflammatory response (Napier et al., 2016; Parnas et al., 2015; Shi et al., 2015b; Zimmermann et al., 2017), and genes required for cell survival, proliferation, and metastasis (Burr et al., 2017; Chen et al., 2015; Fei et al., 2017; Wang et al., 2015; Xu et al., 2017). Practically all these screens measured a single phenotype: cell enrichment or depletion, a single-cell attribute. Such assays are suitable to the pooled format that, with rare exceptions (Cong et al., 2013; Erard et al., 2017), characterizes the vast majority of currently available sgRNA libraries, and enables a relatively facile quantification of the phenotype. Albeit effective and fruitful, the current limitation to single-cell functional assays leaves out collective cell functions which underlie physiologically essential processes. Here we validate a new functional assay we designed to facilitate adaptation of the CRISPR-mediated screen for the identification of genes that regulate the permeability of endothelial cell (EC) monolayers. The integrity of this monolayer is critical to the normal

function of the vascular system because it confers the barrier function of the vessels. Because administration of thrombin produces large gaps in EC monolayers that can be detected with relative ease, we chose to validate the assay by testing if sgRNAs from an existing repressive CRISPR library designed to knockdown the transcription of thrombin pathway genes, are enriched in cells that do not respond to thrombin.

RESULTS

EC monolayers grown on single microcarriers are used as individual permeability assays

We sought an in vitro permeability assay that would be compatible with the high throughput format required for genome-wide screens to interrogate signaling pathways that regulate the integrity of endothelial cell junctions. Currently available permeability assays are not compatible with the requirement of genome-wide screens because they cannot accommodate the large number of samples, and because their multi-well format is unsuitable for the pooled sgRNA libraries used in practically all screens. To our knowledge, the highest sampling capacity currently available for the measurement of paracellular permeability is provided by the 96-well plate filter insert assay format. A comprehensive screen of the human genome by 10 sgRNAs and 5 technical replicates per gene using this assay would require approximately 10^4 multi-well plates, a number that is beyond the capacity of most research laboratories. To design a more suitable assay, we took advantage of the microcarrier (MC)-based cell culture technique developed to maximize the number of adherent cells grown per volume of medium. Typically, MCs consist of spherical beads of a diameter in the range of 100-200 μm, made of cross-linked polymers. Commercially available MCs come in a variety of polymeric matrices and surface treatments or coatings (Martin et al., 2011). MCs carrying EC monolayers had been used to study the effect of various agonists on cell monolayer permeability by measuring the absorbance of dye into the MCs, or in a chromatographic format, by measuring the elution time (Eaton et al., 1991; Killackey et al., 1986; Park et al., 1999; Waters, 1996). In contrast to those approaches, we consider each microcarrier as an individual MAP. This facilitates high throughput testing of a large number of samples in a relatively small volume of growth medium (approximately 4.3×10^5 MCs per 100 mL). We envisioned that ECs will be transduced by either repressive (CRISPRi) or activating (CRISPRa) sgRNA libraries and grown as clonal populations on each MC. When treated by agonists that disrupt cell junction, e.g. vascular endothelial growth factor (VEGF) or thrombin, junctions among ECs expressing sgRNAs that target genes required the for the cellular response to the administered agonist will fail to open up. To distinguish between MCs carrying responsive or non-responsive EC monolayers, we selected a probe that would bind to the MC surface exposed through the gaps between the responsive cells. Since the MC type that supported EC growth optimally is coated with gelatin, we selected the collagen-binding fragment of fibronectin (Owens and Baralle, 1986) because of its high binding affinity to gelatin (Engvall et al., 1978) and conjugated it to a fluorophore. MCs carrying responsive EC monolayers would become fluorescent because of the binding of the fluorescently-conjugated fibronectin fragment to the newly formed gaps between ECs. These MCs would then be separated from those carrying non-responsive monolayers by fluorescence-assisted sorting (Fig. 1).

Thrombin increases the permeability of telomerase-immortalized human primary EC monolayers

Among a variety of known permeability factors, we noted that thrombin induces relatively large openings between confluent ECs (Laposata et al., 1983), as observed also when cells were grown on the same type of MCs used in this study (Killackey et al., 1986). We chose it, therefore, as a convenient agonist for testing MAP validity. To gauge thrombin's effects on the monolayers of the telomerase-immortalized human dermal microvascular ECs (TIME cells) we used throughout this study, we measured thrombin-induced change in permeability by two approaches. In the first, we measured the penetration of a fluorescently-conjugated dextran probe through an EC monolayer. In the second, we measured the thrombin-induced change in the impedance of the monolayer. Both approaches yielded large changes in the measured attributes (Fig. 2A, 2B), indicating substantial increases in monolayer permeability. In the first type of assay, where the measured leakage of the probe is a direct reflection of the formation of pores in the formerly confluent EC monolayer,

the fluorescence of the probe in the lower chamber of the assay increase more than 3-fold (Fig. 2A). In impedance measurements, thrombin concentrations of 0.5, 1.0, and 2.0 U/mL caused a decrease of approximately 1.1 units, although their rate of recovery to the pre-thrombin level was slower as thrombin concentration increased (Fig. 2A). To visualize the structural effects of thrombin on the EC monolayer, we immunolabeled the cells to track the localization of vascular endothelial cadherin (VEcad) and used phalloidin to observe thrombin-induced changes in the actin cytoskeleton. Thrombin induced opening of large gaps, in some locations as large as the width of the ECs (approximately 30 μm), and the formation of denser and thicker stress fibers (Fig. 2C), similar to previous observations (Rabiet et al., 1996).

Single TIME cells grow to confluence on gelatin-coated MCs

Following tests with several types of MC polymers (e.g. polystyrene, diethylaminoethyl dextran), and coatings (e.g. fibronectin, collagen I), we determined that MCs consisting of cross-linked dextran matrix and coated with gelatin are optimal for TIME cell growth. To observe monolayer integrity, we stained them with calcein, a dye that visualized both the cell body and intercellular junctions (Fig, 3A). All the cells grown on each microcarrier in a genome-wide screen are required to express a single sgRNA to avoid mixed effects of silencing the expression of potentially antagonistic genes or additive effects of potentially cooperative genes. Consequently, the TIME cell monolayer on each MC has to evolve from a single cell and form a clonal population. To achieve a 1:1 cell-MC ratio, we seeded one cell per two MCs. Starting from a single cell, TIME cells reached confluence in nine days, forming tightly sealed monolayers like cells grown from an initial larger number (Fig 3B).

TIME cells grown on MCs form intact tight and adherens junctions

Formation of a cobblestone monolayer with integral intercellular junctions is essential for the repurposing of cell-coated MCs as individual permeability assays. Evidence for the establishment of such monolayers on the same type of MCs used here, including at the ultrastructural level, had been reported approximately 30 years ago (Haselton et al., 1989; Killackey et al., 1986). Furthermore, there is no apparent cause that would render formation of intact intercellular junctions less likely on a convex than on a flat surface. Nevertheless, we sought to show that junction-specific proteins are present at the junction of the specific cell type used in this study, as an indication for the integrity of intercellular junction integrity. Tight junctions form a more restrictive barrier than adherens junctions, and do not permit the passage of proteins because of their size-selectivity (Van Itallie et al., 2008). To test their integrity, we immunolabeled JAM-A, a single-pass transmembrane protein and the adaptor protein ZO1, which bind each other in the tight junctions (Ebnet et al., 2000). Confocal microscopy revealed that both proteins were abundantly present at cell borders among all the cells that were visible in the field of view as narrow and undisrupted (Fig. 3C). The adherens junction marker vascular endothelial (VE)-cadherin was similarly abundant and patterned (ibid.). We conclude that the intercellular junctions formed by MAPs do not differ from junctions formed by the same (Fig. 2C) or other (Ngok et al., 2012) ECs.

Thrombin increases attachment of collagen-binding fragment of fibronectin to gelatin-coated surfaces

To assess the compatibility of the fluorophore-conjugated collagen-binding proteolytic fragment of fibronectin (FNc; Fig. 4A), we tested if the extent of its binding to a gelatin-coated substrate depends on EC confluence. The fluorescence signal of the surface-attached probe from MCs with a confluent TIME cell monolayer was miniscule in comparison to the signal of sub-confluent monolayer (Fig 4B). Thrombin treatment of confluent TIME cell layers generated substantial gaps among adjacent cells (Fig 4C). Bare, gelatin-coated MCs bound FNc avidly, whereas MCs coated by a sub-confluent EC monolayer bound only a fraction of the latter (Fig 4D).

Likelihood of false discovery is reduced by removal of non-confluent MCs

Though the majority of TIME cell monolayers reached confluence even when grown from a single cell per MC (Fig. 3B), it is practically impossible to ensure that all MCs are fully coated by cells. Elimination of MCs that have residual exposed surface patches is essential because the FNc probe would bind to these exposed patches, resulting in the misidentification of the cells as intransigent to the sgRNA they were transduced with and responsive to the junction-disrupting agonist during a genome-wide screen. Such an error would result in the omission of potentially relevant genes. To eliminate sub-confluent MCs from the population, we sorted MAPs that were incubated with FNc in the absence of an agonist. We then resorted this group based on MAP peak fluorescence intensity to exclude the least confluent MAPs, whose fluorescence intensity was more than twice of the median intensity (Fig. 5A). This subgroup amounted to 28 percent of the initial total population. To test the efficacy of this approach and the stability of cell monolayers on the MAPs during sorting, we scanned the sorted MAP population. This time, only 10 percent of the input MAPs was detected by the gate used in the first round (Fig. 5B). Visual inspection of a sample from this first group confirmed the presence of exceptionally bright MAPs (Fig. 5C). No exceptionally bright MAPs were detected by visual inspection after sorting (Fig. 5D).

Fluorescence-assisted sorting separates thrombin-treated and untreated TIME cells grown on MCs

Execution of a genome-wide screen requires physical separation between the phenotypes that ensue during the functional assay – in the current study, these are thrombin-responsive and non-responsive MAPs. The conjugation of the FNc probe to a fluorophore would enable separation by fluorescence-assisted sorting (FACS), albeit not by conventional instruments designed to handle cell-sized particles. In order to test the sensitivity of the sorter to the signal of junction disassembly marked by the binding of the FNc probe, compared we fixed the MC-attached TIME cells by EtOH, which is an optimal fixative for the preservation of nucleic acids (Srinivasan et al., 2002), after the assay was completed to prevent changes in cell and junction morphology, and subjected the whole MC population to fluorescence-assisted sorting on a large-bore platform. The target population when using sgRNAs from a CRISPRi library, as in this study, are the MCs on which the cells have not responded to thrombin, presumably due to the repressive effect of the tested sgRNAs. These would be the MCs that emit the lowest fluorescence intensity during sorting, some of which would be detectable only by their optical density, because their fluorescence emission could be lower than the sensitivity of the sorter's light detector. Due to potential disparity in cell response to thrombin, among other conceivable biological variables, the light-intensity distribution of the MC population was not binary, but continuous over an interval between high and low intensity values. We defined two gates, one for the low-responding MCs, referred to as 'negative', and the high-responders that we refer to as 'positive'. The percentage of the population of MCs that were not treated by thrombin and counted as negative fell from approximately 40 percent to only 10 percent of the thrombin-treated MC population (Fig. 6A), due to the upward shift in MC fluorescence intensity. Complementarily, the percentage of positive MCs increased from approximately 15 to 40 percent of the treated MC population (Fig. 6B). These measurements demonstrate a robust and reproducible response to thrombin that can be readily resolved into positive and negative populations. A portion of approximately 45 percent of the total MC population encompassing the medium of the response range remained between the upper and lower gates. This sub-population is least likely to contain MCs carrying cells that express the most repressive sgRNAs. Sidestepping this population was not likely, therefore, to preclude the identification of genes that have major roles in mediating the disassembly of cell junctions in response to thrombin.

sgRNAs repress target gene expression level, protein abundance, and response to thrombin

Execution of a genome-wide screen requires physical separation between the phenotypes that ensue during the functional assay – in the current study, these are the thrombin-responsive and non-responsive TIME-cells. To effectively test if the MC-based permeability assay can achieve this separation by distinguishing

between genes that affect EC response to thrombin, we selected sgRNAs that target *F2R*, the gene that encodes the main thrombin receptor in ECs (Kataoka et al., 2003), as a positive control, and *KDR*, the gene that encodes VEGF receptor 2, the main VEGF receptor in blood vessel ECs (Quinn et al., 1993), as a negative control. We included sgRNAs that target *GNAQ*, a gene encoding $G\alpha_q$, a trimeric GTPase. $G\alpha_q$ mobilizes calcium by activating phospholipase C-β, but unlike $G\alpha_{11/12}$, it is not known to affect EC monolayer permeability (McLaughlin et al., 2005). We selected it, therefore, as an unknown whose effect on the permeability of MC-attached TIME cell monolayers remains to be tested. Before testing the effects of the selected sgRNAs on EC barrier function, we validated the presumed capacity of each of the five individual sgRNAs designed to target single genes (Horlbeck et al., 2016) by measuring how effectively they repressed the transcription of their target genes and, consequently, reduced the abundance of the protein they encode. Using quantitative real-time polymerase chain reaction (qRT-PCR), we detected a large variability among the repressive effects of each set of five sgRNAs that reached more than 13-fold in the case of *F2R*-targeting sgRNAs (Fig. 7A). The most effective one among the five sgRNAs repressed *F2R* transcription to approximately 6 percent of its expression level in TIME cells treated by non-targeting sgRNAs (Fig. 7A). Based on immunoblotting, the pattern of PAR1 abundance in each cell group expressing a single sgRNA fit precisely the qRT-PCR expression pattern of *F2R,* which encodes PAR1. The single sgRNA-specific expression levels of *GNAQ* and *KDR* fit similarly well the abundances of $G\alpha_q$ and *KDR* (Fig. 7B, 7C), confirming that three to four sgRNAs out of each set of five were capable of repressing their target gene by at least 70 percent.

Efficient repression of *F2R* is expected to diminish the effect of thrombin on endothelial cell junctions, which typically lose their interconnections and retract, producing large intercellular gaps (see Fig. 4C). The effect of *GNAQ* repression, on the other hand, remained to be revealed in the planned permeability assays. To test these predictions, we measured the impedance before and after the application of thrombin of TIME cell populations expressing each of the most repressive sgRNAs of *F2R*, *GNAQ*, and *KDR*, grown in multi-well plates. The impedance of TIME cells expressing sgRNAs for *GNAQ*, *KDR*, and a validated negative-control (NC) sgRNA (Horlbeck et al., 2016) fell by close to an impedance unit (Fig. 7D). The impedance of TIME cells expressing *F2R* sgRNA, on the other hand, fell only by 0.2 units and returned to the basal level earlier than the other cell groups.

MAP sensitivity to *F2R* knockdown is similar to impedance measurement

Insufficient sensitivity of a permeability assay may limit severely its utility in general and its capacity to detect genes that modify the response to the tested agonist in particular. We chose impedance measurement as a benchmark for assay sensitivity because this technique is more sensitive than the other major technique based on monolayers cultured on a permeable substrate (Bischoff et al., 2016). To test the sensitivity of impedance measurement as a detector of sgRNA-mediated knockdown of an essential response gene, we compared the response to thrombin of TIME cells transduced by the most effective *F2R*-targeting sgRNA to cells transduced by one of the negative-control sgRNAs. Whereas the impedance of TIME cells transfected by a negative-control sgRNA fell by more than two and a half units, the impedance of TIME cells transfected by a the most effective *F2R*-targeting sgRNA fell only by one unit (Fig. 8A).

As a first step in the test of MAP sensitivity to *F2R* knockdown, we sorted out MAPs whose fluorescence signal was approximately more than double the median intensity of the presorted MAP population. This selection maintained three quarters of the initial population and removed almost entirely the non-confluent MAPs (Fig. 8B). Extinction profiles of individual MAPs show the presence of the gelatin layer and TIME cells coating each MC; fluorescence signal is relatively uniform across the imaged face of each MC. Comparison of histograms of the peak fluorescence of MAPs carrying cells transduced by the most effective *F2R*-targeting sgRNA that were either untreated or treated by thrombin show that thrombin treatment had little effect on the fluorescence distribution of the MAP population (work on the control group is in progress).

F2R sgRNA suppresses thrombin-induced hyperpermeability

All the gene-targeting sgRNAs we tested above repress, albeit to varying degrees, the expression of their target genes. Therefore, we gauged the combined effect of these sgRNAs on MAP permeability by comparing the sorting outcomes of a mixed population made up of equal-sized groups of MAPs carrying cells that express on each MAP one of the 15 sgRNAs employed in the study (five each for *F2R*, *GNAQ*, and *KDR*) to the sorting outcome of MAPs carrying cells that do not express any sgRNA or dCas9-KRAB, as shown in Fig. 6B. The sorting outcome of the first group (Fig. 8D) shows that sgRNA expression almost abolished the population of untreated positive MAPs and reversed the distribution of thrombin-treated MAPs. The former was more than halved, and the latter increased by close to seven-fold. These large effects demonstrate the repressive efficacy of the combined group of sgRNAs. To visualize the individual effect of the most repressive *F2R*, *GNAQ* and *KDR*-targeted sgRNAs in comparison to three validated NC sgRNAs (Horlbeck et al., 2016) on MAP permeability, we imaged the fluorescence of thrombin-treated MAPs with each of these sgRNAs. Cells expressing either *GNAQ*, or *KDR*-targeted sgRNAs responded to thrombin similarly to the negative-control sgRNA-expressing MCs (Fig. 8E). In contrast, the response of MAPs with cells that expressed the most effective *F2R* sgRNA was similar to that of MAPs carrying untreated cells that expressed one of the (top row of images in Fig. 8F) negative-control sgRNAs. These results are consistent with the rest of the functional effects of the sgRNAs. The persistence of low light intensity emitted by MCs carrying cell that express a *F2R* sgRNA indicate that thrombin treatment did not cause an artifactual signal resulting from cell detachment from the MC surface. Moreover, since the sorting is to be used in combination with an inhibitory library, it separates the MCs that emit the lowest light signal. Therefore, artifactually bright MCs cannot cause false gene identification.

DISCUSSION

In contrast to most if not all genetic screens performed to date, the new assay facilitates genetic screens of a collective cell function. Previous screens measured phenotypes that reflect changes in cell number, an activity of individual cells. Permeability is not amenable to existing functional assays, because it is inherently a collective cell function. The new assay repurposes a pre-existing device – microspheres that had been developed over fifty years ago to increase the surface available for the growth of adherent cells (van Wezel, 1967). MCs had already been used, in fact, to measure EC monolayer permeability, albeit in bulk format (Killackey et al., 1986). In contrast, the new assay deploys each cell-coated microcarrier as a single sample, thus taking advantage of the small MC diameter, 150 μm on the average, to pack as many as 6000 MCs per mL of medium. At this sample concentration, 166 mL of growth medium would contain 10^6 MCs. As estimated above, this is a sufficiently large number of samples for performing a genome-wide screen.

Screens based on cell growth can measure a continuum of quantitative phenotypes by counting the numbers of cells that express sgRNAs of interest (Kampmann et al., 2013). These measurements can be used for further analysis of the targets identified in the first screen, such as construction of genetic interaction (GI) maps (Bassik et al., 2013). Though the phenotypes of the MCs (i.e., their fluorescence intensities), also vary continuously within a certain range, the sorting converts that range into an either “positive” or “negative” binary output, precluding the attribution of a continuous range of quantitative phenotypes to each sample, and further analysis. This drawback can be overcome, however, by performing a set of replicate assays where the position of the gate is changed incrementally so that a larger range of phenotypes is sampled. Replicating the assay is straightforward because it can be run in as little as 30 min using a volume of less than 200 mL MCs in growth medium.

In addition to compactness, the format of the assay facilitates physical separation between samples that are either responsive or refractory to the stimulus by using the phenotype as a sorting input. The separation is crucial for the identification of the genes that produce the measured phenotype. Counting the number of cells on the MCs, and determining if the cell monolayer reached confluence are straightforward because the cells

on the MC surface can be readily visualized by a dye and by other imaging modalities (Haselton et al., 1989; Killackey et al., 1986). The visibility enables growth of a clonal cell population from a single cell per MC, and makes it possible to verify that the cell monolayer coating the MCs is confluent, preventing spurious signal as a result of probe binding to the exposed surface of the MC. The duration of the assay, i.e. the time necessary for eliciting a measurable phenotype depends on the nature of the agonist, but it is not likely to allow sufficient time for the emergence of multiple phenotypes, such as change in cell density. This narrows the scope of the assay to its intended purpose of measuring intercellular permeability and prevents interference from other potential effects of the agonists which are often pleiotropic, such as thrombin. While the assay was validated by thrombin-induced hyperpermeability of EC monolayers, it is compatible with any monolayer-forming cell type, such as epithelial cells, and with any agonist that induces disruption of intercellular junctions.

Screening an untreated cell population that expresses a CRISPi library would be potentially productive beyond the removal of MCs that carry non-confluent TIME cell monolayers. It is conceivable that the homeostasis of intercellular junctions requires the activity and turnover of certain proteins. At least some of the non-confluent MCs may carry clonal cell populations that express sgRNAs which knockdown genes that encode these proteins. Their identification could be as significant as that of genes that encode proteins which are required for the response to junction-disrupting agonists.

MATERIALS AND METHODS

Endothelial cell culture

Telomerase-immortalized microvascular endothelial (TIME) cells (American Type Cell Culture) were grown at 37°C in a humidified 5 percent CO_2 incubator in Vascular Cell Basal Medium supplemented with Microvascular Endothelial growth Kit-VEGF (ATCC) and 12.5 µg/mL blasticidin (ThermoFisher Scientific).

Immunofluorescence

TIME cells grown to confluence on gelatin-coated round 12-mm glass coverslips (GG-12-Gelatin, Neuvitro) were treated with 2 U/mL thrombin (human α-thrombin, Enzyme Research Laboratories), for 30 min at 37°C, and 5 percent CO_2, or with PBS as a negative control. After washing in ice-cold PBS, fixation in 4 percent paraformaldehyde/PBS for 30 min at 23°C, and permeabilization in 0.1 percent Triton X-100 (Sigma-Aldrich) in PBS for 5 min, cells were incubated in a blocking solution of 5 percent bovine serum albumin (BSA, Sigma-Aldrich) in PBS for 1 h. Immunolabeling by primary antibodies diluted according to the manufacturer's instruction in 0.1 percent Triton X-100, 1 percent BSA, in PBS overnight at 4 °C was followed by a 3×PBS wash and incubation with fluorescently-conjugated secondary antibodies at 2.5 µg/mL in PBS for 30 min at 23°C. After a 3×PBS wash, coverslips were mounted on glass slides (ProLong Gold Antifade Mountant, ThermoFisher Scientific). Images of TIME cells grown either as a two-dimensional culture or on MCs were acquired by epi-fluorescence microscopy (EVOS FL Auto Cell Imaging System, ThermoFisher Scientific).

Immunoblotting

Cells were scraped off plates, lysed in on in RIPA lysis buffer (25 mM Tris-HCl pH 7.6, 150mM NaCl, 1 percent NP-40, 1 percent sodium deoxycholate, 0.1 percent SDS; ThermoFisher Scientific) supplemented with phosphatase (Fisher Scientific) and protease (Sigma-Aldrich) inhibitor cocktails, and clarified by centrifugation (20,000 g, 10 min). Total protein concentration was determined by BCA protein assay (ThermoFisher Scientific). Equal amounts of total protein were separated by 10 percent SDS-PAGE and transferred to a PVDF membrane. Membranes were blocked by 5 percent casein in TBS with 0.1 percent Tween 20, probed with the indicated primary antibodies, and incubated with HRP-conjugated secondary antibodies for 1 h at 23°C. Protein-antibody complexes were visualized by chemiluminescence (SuperSignal™ West Pico PLUS, ThermoFisher Scientific) on film (HyBlot CL® Autoradiography Film, Denville Scientific Inc.).

Impedance measurement

Impedance was measured on xCELLigence Real-Time Cell Analyzer (RTCA; ACEA Biosc.) according to the manufacturer's instructions. Briefly, 30000 TIME cells were seeded in 200 µL growth medium per well of an electronic 16-well plate (E-Plate VIEW 16, ACEA Biosc.) for 30 min at 23°C to allow cell sedimentation. The cells were grown to confluence at 37°C, 5 percent CO_2. On the day of experiment, cells were treated by thrombin or by the same volume of carrier (PBS), and placed in the analyzer for continuous recording of impedance during the next 24 hours. Relative impedance is expressed as $(Z_i-Z_0)/15\ \Omega$, where Z_i is the impedance at the ith time point, and Z_0 is the initial impedance before the addition of thrombin.

Macromolecular permeability

TIME cells seeded at 1×10^5 per filter insert (0.4 µm pores, 6.4 mm diameter, polyethylene terephthalate membrane, Transwell®, Corning) were grown for 72 h in 24-well plates (Transwell®, Corning) filled with 800 µL growth medium per well. The cells in the inserts were supplemented at the same time by either 2 U/mL thrombin or carrier, and by 1 µg/mL fluorescein isothiocyanate (FITC)-dextran (2000 kDa, Sigma-Aldrich) was added in the upper chamber. 10 µL samples were taken after 0, 5, 15, 30, 60, 90 and 120 min from the lower

compartment. The removed samples were diluted in 90 μL of PBS, transferred in a 96 well black plate, clear bottom and fluorescence measured with a fluorimeter (Ex/Em: 485/535 nm VICTOR^2, PerkinElmer). Results are expressed as arbitrary light intensity counts.

TIME cell culture on microcarriers in spinner flasks

Cytodex 3 MCs (GE Health Sciences) were hydrated at 50 mL/g in PBS for 3 h at room temperature, washed twice at 30 mL/g in PBS, and autoclaved (121°C, 20 min). A quantity of 92 mg Cytodex 3 MCs were readied for cell growth by incubation overnight at 37°C, 5 percent CO_2 and stirred at 35 rpm (Troemner) in 50 mL growth medium in 100 mL siliconized (Sigmacote, Sigma-Aldrich) spinner flasks (Bellco Glass, model 1965-95010) equipped with glass-ball. TIME cells grown to 80 percent confluence in T75 flasks were briefly detached with 0.05 percent trypsin, 0.02 percent EDTA (ATCC). The cells were then resuspended in growth medium supplemented with 15 percent FBS and 4.5 g/L glucose (supplemented growth medium). Spent medium was replace in the spinner flasks with 30 mL of fresh supplemented growth medium, MCs were inoculated with $6X10^6$ cells and the volume was completed to 50 mL of supplemented growth medium to achieve a density of 24000 cells/cm^2. The MC culture was incubated at 37°C, 5 percent CO_2 and stirred intermittently for 1 min every 15 min for 1 hour at 35 rpm, then stirred continuously at 35 rpm. The medium was replenished once every two days by exchanging 50 mL with fresh medium. The cells reached confluence in 3-5 days. In order to start with the attachment of 1 cell per MC, MCs were inoculated with $1.5X10^5$ cells and the volume was completed to 50 mL of growth medium to achieve a density of 600 cells/cm^2. To monitor cell growth on MCs, a small MC sample was removed every day, treated with 2 μM of Calcein AM (ThermoFisher Scientific), and visualized with fluorescent microscope. Under these conditions, cells reached confluence in 9 days.

Detection of barrier disruption by fluorophore-conjugated fragment of fibronectin

To detect disruption of the confluent TIME cell monolayer grown on MCs, we used a 45 kDa fibronectin proteolytic fragment (FNc, Sigma-Aldrich) purified from human plasma (Sigma-Aldrich) conjugated to Dylight 550 with a labeling kit (ThermoFisher Scientific). This fluorescently-conjugated FNc is able to bind to the newly gelatin-coated surface exposed between neighboring cells. TIME cells were grown to confluence on gelatin-coated round 12-mm diameter glass coverslips (GG-12-Gelatin, Neuvitro). On the day of permeability assay, TIME cells were treated with thrombin for 30 min at 2 U/mL and with 1 μg/mL FNc for 5 min. The cells were then washed with ice cold PBS, fixed in 4 percent paraformaldehyde/PBS for 30 min, and washed again with PBS. The coverslips were mounted on glass slides with Prolong Gold (Invitrogen), a DAPI-containing medium. Permeability was characterized by the red fluorescence (Ex/Em: 562⁄576 nm) of the dye Dylight 550 after taking pictures with a fluorescent microscope.

Permeability assay using Thrombin on cytodex3 microcarriers

TIME cells grown to confluence on MCs were incubated with 2 U/mL of Thrombin for 25 min while stirring at 35 rpm at 37°C, 5 percent CO_2. The medium was then supplemented with 1 μg/mL Dylight 550-conjugated FN (FNc) and stirred for 5 min. MCs were transferred into a plate for visualization and characterization of the red fluorescence of the Dylight 550 dye by the EVOS FL microscope.

Microcarrier sorting

Cells grown on MCs and treated as desired were fixed by 50 percent EtOH/PBS/1 percent FBS for 10 min at room temperature, washed twice in 70 percent EtOH/PBS/1 percent FBS for 10 min at 4°C, then transferred to PBS/1 percent FBS. MC samples were analyzed based on their time of flight and fluorescence intensity at 561 nm using a Biosorter (Union Biometrica) equipped with a FP-1000 1000 μm flow cells. MCs were then sorted by Biosorter, based on user-defined fluorescence intensity gates (“negative” or “positive”).

DNA extraction from microcarrier-attached TIME cells

TIME cells were lysed on the MCs by the lysis buffer of the DNA extraction kit (Nucelospin Blood, Macherey-Nagel). DNA was extracted from the cell lysate following the manufacturer's instructions.

Expression of *dCas9-KRAB* and repressive sgRNAs in TIME cells and genomic DNA sequencing

Lentiviri were produced and infected into TIME cells as described (Kampmann et al., 2014). The cells were transduced first by lentivirus expressing inactive Cas9 fused to the KRAB repressor module (Gilbert et al., 2014) (pHR-SFFV-dCas9-BFP-KRAB, Addgene). Lentivirus-expressing cells were sorted (FACSAria II, BD Biosciences) using blue fluorescent protein (BFP) as a marker. Oligonucleotides encoding five optimized sgRNAs targeting the transcription start sites of *F2R*, *GNAQ*, and *KDR* and NC sgRNAs were synthesized based on sequences from the CRISPRi V2 library designed by Horlbeck et al. (Horlbeck et al., 2016). Each sgRNA was subcloned into the backbone plasmid of the CRISPRi V2 library (pU6-sgRNA EF1Alpha-puro-T2A-BFP, Addgene) between the BstXI and BlpI restriction sites. Groups of *dCas9-KRAB*-expressing TIME cells were each infected separately by lentiviri expressing a single sgRNA and selected by puromycin resistance conferred by the sgRNA-expressing plasmid. The presence of sgRNAs in the genomes of TIME cells adhered to sorted MCs were quantified by qRT-PCR using a forward primer based on the sequence of the backbone plasmid of the sgRNA library, pU6-sgRNA EF1Alpha-puro-T2A-BFP, and a reverse primer specific to each sgRNA. The sequences are provided in supplementary Table 1.

Statistics

The significance of the difference between means was determined by two-tailed Student's *t*-test. The null hypothesis was considered untrue if the probability satisfied the condition $P \leq 0.05$.

ACKNOWLEDGMENTS

We thank Dr. Florin Tuluc, Flow Cytometry Core Laboratory of the Children's Hospital of Philadelphia, for assistance in FACS; Drs. Luke Gilbert and Max Horlbeck, and by Ryan Pak, for assistance in the use of the CRISPR/dCas9 library developed in the lab of Dr. Jonathan Weissman, University of California, San Francisco.

This study was supported by the National Heart Lung and Blood Institute (R01 grant HL119984 to AH and R01 grant HL128234 to LE) and by the National Cancer Institute (P30 grant CA56036 to PF).

Author contributions: CS designed and performed experiments, analyzed the results, and wrote the manuscript; JY and XK performed experiments, analyzed the results, and prepared reagents; RK performed experiments, LE supervised the preparation of reagents and designed experiments; PF supervised the preparation of reagents and DNA sequencing, and analyzed data; EL designed experiments, analyzed data, and wrote the manuscript; AH conceived the study, coordinated its performance, designed experiments, analyzed the results, and wrote the manuscript.

The authors have no competing financial interests.

REFERENCES

Adamson, B., T.M. Norman, M. Jost, M.Y. Cho, J.K. Nunez, Y. Chen, J.E. Villalta, L.A. Gilbert, M.A. Horlbeck, M.Y. Hein, R.A. Pak, A.N. Gray, C.A. Gross, A. Dixit, O. Parnas, A. Regev, and J.S. Weissman. 2016. A Multiplexed Single-Cell CRISPR Screening Platform Enables Systematic Dissection of the Unfolded Protein Response. *Cell*. 167:1867-1882 e1821.

Bassik, M.C., M. Kampmann, R.J. Lebbink, S. Wang, M.Y. Hein, I. Poser, J. Weibezahn, M.A. Horlbeck, S. Chen, M. Mann, A.A. Hyman, E.M. Leproust, M.T. McManus, and J.S. Weissman. 2013. A systematic mammalian genetic interaction map reveals pathways underlying ricin susceptibility. *Cell*. 152:909-922.

Bischoff, I., M.C. Hornburger, B.A. Mayer, A. Beyerle, J. Wegener, and R. Furst. 2016. Pitfalls in assessing microvascular endothelial barrier function: impedance-based devices versus the classic macromolecular tracer assay. *Sci Rep*. 6:23671.

Burr, M.L., C.E. Sparbier, Y.C. Chan, J.C. Williamson, K. Woods, P.A. Beavis, E.Y.N. Lam, M.A. Henderson, C.C. Bell, S. Stolzenburg, O. Gilan, S. Bloor, T. Noori, D.W. Morgens, M.C. Bassik, P.J. Neeson, A. Behren, P.K. Darcy, S.J. Dawson, I. Voskoboinik, J.A. Trapani, J. Cebon, P.J. Lehner, and M.A. Dawson. 2017. CMTM6 maintains the expression of PD-L1 and regulates anti-tumour immunity. *Nature*. 549:101-105.

Chavez, A., M. Tuttle, B.W. Pruitt, B. Ewen-Campen, R. Chari, D. Ter-Ovanesyan, S.J. Haque, R.J. Cecchi, E.J.K. Kowal, J. Buchthal, B.E. Housden, N. Perrimon, J.J. Collins, and G. Church. 2016. Comparison of Cas9 activators in multiple species. *Nat Methods*. 13:563-567.

Chen, S., N.E. Sanjana, K. Zheng, O. Shalem, K. Lee, X. Shi, D.A. Scott, J. Song, J.Q. Pan, R. Weissleder, H. Lee, F. Zhang, and P.A. Sharp. 2015. Genome-wide CRISPR screen in a mouse model of tumor growth and metastasis. *Cell*. 160:1246-1260.

Cong, L., F.A. Ran, D. Cox, S. Lin, R. Barretto, N. Habib, P.D. Hsu, X. Wu, W. Jiang, L.A. Marraffini, and F. Zhang. 2013. Multiplex genome engineering using CRISPR/Cas systems. *Science*. 339:819-823.

Eaton, B.M., V.J. Toothill, H.A. Davies, J.D. Pearson, and G.E. Mann. 1991. Permeability of human venous endothelial cell monolayers perfused in microcarrier cultures: effects of flow rate, thrombin, and cytochalasin D. *J Cell Physiol*. 149:88-99.

Ebnet, K., C.U. Schulz, M.K. Meyer Zu Brickwedde, G.G. Pendl, and D. Vestweber. 2000. Junctional adhesion molecule interacts with the PDZ domain-containing proteins AF-6 and ZO-1. *J Biol Chem*. 275:27979-27988.

Engvall, E., E. Ruoslahti, and E.J. Miller. 1978. Affinity of fibronectin to collagens of different genetic types and to fibrinogen. *J Exp Med*. 147:1584-1595.

Erard, N., S.R.V. Knott, and G.J. Hannon. 2017. A CRISPR Resource for Individual, Combinatorial, or Multiplexed Gene Knockout. *Mol Cell*. 67:348-354 e344.

Fei, T., Y. Chen, T. Xiao, W. Li, L. Cato, P. Zhang, M.B. Cotter, M. Bowden, R.T. Lis, S.G. Zhao, Q. Wu, F.Y. Feng, M. Loda, H.H. He, X.S. Liu, and M. Brown. 2017. Genome-wide CRISPR screen identifies HNRNPL as a prostate cancer dependency regulating RNA splicing. *Proc Natl Acad Sci U S A*. 114:E5207-E5215.

Gayle, S., S. Landrette, N. Beeharry, C. Conrad, M. Hernandez, P. Beckett, S.M. Ferguson, T. Mandelkern, M. Zheng, T. Xu, J. Rothberg, and H. Lichenstein. 2017. Identification of apilimod as a first-in-class PIKfyve kinase inhibitor for treatment of B-cell non-Hodgkin lymphoma. *Blood*. 129:1768-1778.

Gilbert, L.A., M.A. Horlbeck, B. Adamson, J.E. Villalta, Y. Chen, E.H. Whitehead, C. Guimaraes, B. Panning, H.L. Ploegh, M.C. Bassik, L.S. Qi, M. Kampmann, and J.S. Weissman. 2014. Genome-Scale CRISPR-Mediated Control of Gene Repression and Activation. *Cell*. 159:647-661.

Haselton, F.R., S.N. Mueller, R.E. Howell, E.M. Levine, and A.P. Fishman. 1989. Chromatographic demonstration of reversible changes in endothelial permeability. *J Appl Physiol (1985)*. 67:2032-2048.

Horlbeck, M.A., L.A. Gilbert, J.E. Villalta, B. Adamson, R.A. Pak, Y. Chen, A.P. Fields, C.Y. Park, J.E. Corn, M. Kampmann, and J.S. Weissman. 2016. Compact and highly active next-generation libraries for CRISPR-mediated gene repression and activation. *Elife*. 5.

Kampmann, M., M.C. Bassik, and J.S. Weissman. 2013. Integrated platform for genome-wide screening and construction of high-density genetic interaction maps in mammalian cells. *Proc Natl Acad Sci U S A*. 110:E2317-2326.

Kampmann, M., M.C. Bassik, and J.S. Weissman. 2014. Functional genomics platform for pooled screening and generation of mammalian genetic interaction maps. *Nat Protoc*. 9:1825-1847.

Kataoka, H., J.R. Hamilton, D.D. McKemy, E. Camerer, Y.W. Zheng, A. Cheng, C. Griffin, and S.R. Coughlin. 2003. Protease-activated receptors 1 and 4 mediate thrombin signaling in endothelial cells. *Blood*. 102:3224-3231.

Kearns, N.A., R.M. Genga, M.S. Enuameh, M. Garber, S.A. Wolfe, and R. Maehr. 2014. Cas9 effector-mediated regulation of transcription and differentiation in human pluripotent stem cells. *Development*. 141:219-223.

Killackey, J.J., M.G. Johnston, and H.Z. Movat. 1986. Increased permeability of microcarrier-cultured endothelial monolayers in response to histamine and thrombin. A model for the in vitro study of increased vasopermeability. *Am J Pathol*. 122:50-61.

Konermann, S., M.D. Brigham, A.E. Trevino, J. Joung, O.O. Abudayyeh, C. Barcena, P.D. Hsu, N. Habib, J.S. Gootenberg, H. Nishimasu, O. Nureki, and F. Zhang. 2015. Genome-scale transcriptional activation by an engineered CRISPR-Cas9 complex. *Nature*. 517:583-588.

Kurata, M., S.K. Rathe, N.J. Bailey, N.K. Aumann, J.M. Jones, G.W. Veldhuijzen, B.S. Moriarity, and D.A. Largaespada. 2016. Using genome-wide CRISPR library screening with library resistant DCK to find new sources of Ara-C drug resistance in AML. *Sci Rep*. 6:36199.

Laposata, M., D.K. Dovnarsky, and H.S. Shin. 1983. Thrombin-induced gap formation in confluent endothelial cell monolayers in vitro. *Blood*. 62:549-556.

Manguso, R.T., H.W. Pope, M.D. Zimmer, F.D. Brown, K.B. Yates, B.C. Miller, N.B. Collins, K. Bi, M.W. LaFleur, V.R. Juneja, S.A. Weiss, J. Lo, D.E. Fisher, D. Miao, E. Van Allen, D.E. Root, A.H. Sharpe, J.G. Doench, and W.N. Haining. 2017. In vivo CRISPR screening identifies Ptpn2 as a cancer immunotherapy target. *Nature*. 547:413-418.

Martin, Y., M. Eldardiri, D.J. Lawrence-Watt, and J.R. Sharpe. 2011. Microcarriers and their potential in tissue regeneration. *Tissue Eng Part B Rev*. 17:71-80.

McLaughlin, J.N., L. Shen, M. Holinstat, J.D. Brooks, E. Dibenedetto, and H.E. Hamm. 2005. Functional selectivity of G protein signaling by agonist peptides and thrombin for the protease-activated receptor-1. *J Biol Chem*. 280:25048-25059.

Napier, B.A., S.W. Brubaker, T.E. Sweeney, P. Monette, G.H. Rothmeier, N.A. Gertsvolf, A. Puschnik, J.E. Carette, P. Khatri, and D.M. Monack. 2016. Complement pathway amplifies caspase-11-dependent cell death and endotoxin-induced sepsis severity. *J Exp Med*. 213:2365-2382.

Ngok, S.P., R. Geyer, M. Liu, A. Kourtidis, S. Agrawal, C. Wu, H.R. Seerapu, L.J. Lewis-Tuffin, K.L. Moodie, D. Huveldt, R. Marx, J.M. Baraban, P. Storz, A. Horowitz, and P.Z. Anastasiadis. 2012. VEGF and Angiopoietin-1 exert opposing effects on cell junctions by regulating the Rho GEF Syx. *J Cell Biol*. 199:1103-1115.

Owens, R.J., and F.E. Baralle. 1986. Mapping the collagen-binding site of human fibronectin by expression in Escherichia coli. *EMBO J*. 5:2825-2830.

Park, J.H., N. Okayama, D. Gute, A. Krsmanovic, H. Battarbee, and J.S. Alexander. 1999. Hypoxia/aglycemia increases endothelial permeability: role of second messengers and cytoskeleton. *Am J Physiol*. 277:C1066-1074.

Parnas, O., M. Jovanovic, T.M. Eisenhaure, R.H. Herbst, A. Dixit, C.J. Ye, D. Przybylski, R.J. Platt, I. Tirosh, N.E. Sanjana, O. Shalem, R. Satija, R. Raychowdhury, P. Mertins, S.A. Carr, F. Zhang, N. Hacohen, and A. Regev. 2015. A Genome-wide CRISPR Screen in Primary Immune Cells to Dissect Regulatory Networks. *Cell*. 162:675-686.

Quinn, T.P., K.G. Peters, C. De Vries, N. Ferrara, and L.T. Williams. 1993. Fetal liver kinase 1 is a receptor for vascular endothelial growth factor and is selectively expressed in vascular endothelium. *Proc Natl Acad Sci U S A*. 90:7533-7537.

Rabiet, M.J., J.L. Plantier, Y. Rival, Y. Genoux, M.G. Lampugnani, and E. Dejana. 1996. Thrombin-induced increase in endothelial permeability is associated with changes in cell-to-cell junction organization. *Arterioscler Thromb Vasc Biol*. 16:488-496.

Shi, J., E. Wang, J.P. Milazzo, Z. Wang, J.B. Kinney, and C.R. Vakoc. 2015a. Discovery of cancer drug targets by CRISPR-Cas9 screening of protein domains. *Nat Biotechnol*. 33:661-667.

Shi, J., Y. Zhao, K. Wang, X. Shi, Y. Wang, H. Huang, Y. Zhuang, T. Cai, F. Wang, and F. Shao. 2015b. Cleavage of GSDMD by inflammatory caspases determines pyroptotic cell death. *Nature*. 526:660-665.

Srinivasan, M., D. Sedmak, and S. Jewell. 2002. Effect of fixatives and tissue processing on the content and integrity of nucleic acids. *Am J Pathol*. 161:1961-1971.

Tao, L., J. Zhang, P. Meraner, A. Tovaglieri, X. Wu, R. Gerhard, X. Zhang, W.B. Stallcup, J. Miao, X. He, J.G. Hurdle, D.T. Breault, A.L. Brass, and M. Dong. 2016. Frizzled proteins are colonic epithelial receptors for C. difficile toxin B. *Nature*. 538:350-355.

Thakore, P.I., A.M. D'Ippolito, L. Song, A. Safi, N.K. Shivakumar, A.M. Kabadi, T.E. Reddy, G.E. Crawford, and C.A. Gersbach. 2015. Highly specific epigenome editing by CRISPR-Cas9 repressors for silencing of distal regulatory elements. *Nat Methods*. 12:1143-1149.

Van Itallie, C.M., J. Holmes, A. Bridges, J.L. Gookin, M.R. Coccaro, W. Proctor, O.R. Colegio, and J.M. Anderson. 2008. The density of small tight junction pores varies among cell types and is increased by expression of claudin-2. *J Cell Sci*. 121:298-305.

van Wezel, A.L. 1967. Growth of cell-strains and primary cells on micro-carriers in homogeneous culture. *Nature*. 216:64-65.

Wang, T., K. Birsoy, N.W. Hughes, K.M. Krupczak, Y. Post, J.J. Wei, E.S. Lander, and D.M. Sabatini. 2015. Identification and characterization of essential genes in the human genome. *Science*. 350:1096-1101.

Waters, C.M. 1996. Flow-induced modulation of the permeability of endothelial cells cultured on microcarrier beads. *J Cell Physiol*. 168:403-411.

Xu, C., X. Qi, X. Du, H. Zou, F. Gao, T. Feng, H. Lu, S. Li, X. An, L. Zhang, Y. Wu, Y. Liu, N. Li, M.R. Capecchi, and S. Wu. 2017. piggyBac mediates efficient in vivo CRISPR library screening for tumorigenesis in mice. *Proc Natl Acad Sci U S A*. 114:722-727.

Yamauchi, T., T. Masuda, M.C. Canver, M. Seiler, Y. Semba, M. Shboul, M. Al-Raqad, M. Maeda, V.A.C. Schoonenberg, M.A. Cole, C. Macias-Trevino, Y. Ishikawa, Q. Yao, M. Nakano, F. Arai, S.H. Orkin, B. Reversade, S. Buonamici, L. Pinello, K. Akashi, D.E. Bauer, and T. Maeda. 2018. Genome-wide CRISPR-Cas9 Screen Identifies Leukemia-Specific Dependence on a Pre-mRNA Metabolic Pathway Regulated by DCPS. *Cancer Cell*.

Zimmermann, S., L. Pfannkuch, M.A. Al-Zeer, S. Bartfeld, M. Koch, J. Liu, C. Rechner, M. Soerensen, O. Sokolova, A. Zamyatina, P. Kosma, A.P. Maurer, F. Glowinski, K.P. Pleissner, M. Schmid, V. Brinkmann, A. Karlas, M. Naumann, M. Rother, N. Machuy, and T.F. Meyer. 2017. ALPK1- and TIFA-Dependent Innate Immune Response Triggered by the Helicobacter pylori Type IV Secretion System. *Cell Rep*. 20:2384-2395.

FIGURE LEGENDS

Figure 1: Microcarriers are repurposed as miniature individual permeability assays. A. Gelatin-coated MCs composed of cross-linked dextran carry a confluent EC monolayer (green, to designate calcein-loaded ECs, as shown in Figs. 3 and 5), incubated in medium containing the collagen-binding proteolytic fragment of fibronectin conjugated to a fluorophore (FNc). Once treated by a junction-disrupting agonist (thrombin in this study), FNc binds to the exposed gelatin surface between cells whose junctions disassembled in response to the agonist. **B.** MCs carrying untreated ECs bind a minimal amount of FNc. MCs carrying agonist-treated ECs bind varying amounts of FNc, depending on the identity of the gRNA expressed by the clonal cell population on each MC. MCs carrying ECs that express gRNAs targeting genes that encode proteins required for the induction of the disassembly of cell-cell junctions bind a low amount FNc, similar to untreated MCs. ECs expressing gRNAs that are unrelated to the signaling pathway of the junction-disrupting agonist respond by disassembling their junctions. FNc binds to the gelatin surface exposed between the responsive ECs, rendering the MCs that carry these cells fluorescent. The fluorescent MCs and the dark MCs are separated by fluorescence assisted sorting. The gates of the sorting machine can be set up to capture any group of interest in this population, based on the fluorescence intensity of the MCs of interest.

Figure 2: Thrombin increases the paracellular permeability of TIME cell monolayers. A. Epifluorescence images of confluent TIME cells in monolayers grown on gelatin-coated coverslips. Intercellular junctions disassembled upon treatment by 2 U/mL thrombin (Thr), as indicated by the change in the VEcad signal. The cells formed thicker stress fibers and detached from each other (UT, untreated). **B.** The permeability of TIME cell confluent monolayers grown on filter inserts to 2000 kDa FITC-dextran increased in response to treatment by 2.0 U thrombin, as indicated by the augmentation of the fluorescence signal from the bottom well under the filter. **C.** The impedance of TIME cell monolayers grown on electrodes embedded in the bottom of multi-well plates fell sharply after treatment by the listed dosages of thrombin, indicating that the integrity of the monolayer deteriorated.

Figure 3: TIME cells form a clonal confluent cobble-stone monolayer on MCs. A. Images of calcein AM-stained TIME cells seeded on MCs at a density of 1.5×10^4 cells/cm^2 MC surface area and grown for the indicated durations in spinner flasks. The cells reached confluence after 4 days and formed a tightly-sealed monolayer (see cell junctions in inset). Scale bars, 200 (top row) and 100 (bottom row) μm. **B.** When initiated from a single TIME cell per MC, a confluent monolayer was formed in 9 days. The inset visualizes intercellular junctions. Scale bar, 100 μm.

Figure 4: FNc identifies gaps between thrombin-treated confluent TIME cells. A. Scheme of human fibronectin showing the location of the collagen-binding domain. **B**. TIME cells grown on gelatin-coated glass coverslip until reaching the indicated confluences were incubated with 1 μg/mL FNc (red) for 5 min. Scale bar, 100 μm. **C.** Confluent TIME cells grown as described above were either untreated (UT) or treated by 2 U/mL thrombin (Thr) for 30 min followed by incubation with 1 μg/mL FNc for 5 m. **D.** MCs without cells or MCs carrying TIME cells at the indicated confluence were treated with 1 μg/mL FNc for 30 minutes. Scale bar, 200 μm.

Figure 5. Binding of FNc removes non-confluent MAPs. A. Density plot of MAP extinction per time-of-flight of the untreated MAP population that was incubated with FNc prior to sorting, and histogram showing the gate placed at approximately 2-fold intensity of the median peak of MAP fluorescence intensity. **B.** Density plot of the sorted MAP population and histogram showing MAP counts per their peak fluorescence intensities. **C.** Image of a group of presorted MAPs showing the fluorescence of bound FNc. **D.** A similar image of a group of sorted MAPs (scale bar, 1 mm).

Figure 6. Dark and fluorescent MCs are over-abundant in untreated or thrombin-treated populations, respectively. A. Confluent TIME cells grown on MCs were either untreated or treated by 2 U/mL thrombin for 30 min followed by 5 min incubation with 1 μg/mL FNc for 5 min. The cells were then fixed on MCs by 60 percent EtOH prior to sorting (Time of flight). **B**. Negative and positive populations of microcarriers were represented on a histogram among each sample.

Figure 7. Highly effective sgRNAs reduce substantially the expression and abundance of the targeted gene and encoded protein, respectively. A. Quantification of qRT-PCR measurements of the expression levels of *F2R* in TIME cells transduced by each one of the five CRISPRi library sgRNAs that target *F2R* (mean±SD, n=3). The immunoblot (one of duplicate experiments) on the right side shows PAR1 abundance in TIME cells transduced by the same sgRNAs. **B** and **C**. The same measurements as above for the sgRNAs that target *GNAQ* or *KDR*.

Figure 8. *F2R* sgRNA suppresses thrombin-induced hyperpermeability. A. Time course of impedance measurements of thrombin-treated normalized TIME cells relative to the impedance of untreated ones, expressing NC-2 sgRNA. Each trace represents 3 samples on a multi-well plate. **B.** Density plot of peak fluorescence of a presorted population of MAPs that carry cells transduced by *F2R*-targeting sgRNA showing the sorting gate; a histogram showing counts per peak fluorescence of the sorted MAPs gated in respect to the density plot; a quadruplet of individual MAP emission and extinction profiles. **C.** Histograms showing counts per peak fluorescence of sorted MAPs that carry cells transduced by *F2R*-targeting sgRNA, either untreated or treated by thrombin. **D.** Effects of thrombin treatment on the fluorescence intensity of MAPs carrying TIME cell transduced by the indicated sgRNAs. **E.** Percentages of MAPs sorted from a population consisting of equal numbers of MAPs of cells transduced by each of the18 sgRNAs employed in the study (five each for *F2R*, *GNAQ*, and *KDR*, and three negative-control sgRNAs) under the indicated conditions (mean±SD, n=4). **F.** Triplicate fluorescence images of the MAPs carrying cells transduced by the indicated sgRNAs, under the indicated conditions. Scale bar, 100 μm.

SUPPLEMENTARY MATERIAL

The supplementary material consists of one Excel files that contains one table.

Table S1: Sequences of the sgRNAs from the CRISPRi V2 library (Horlbeck et al., 2016), the sgRNA-specific reverse primers used in qRT-PCR experiments, and the forward primer based on the sequence of the backbone plasmid of the sgRNA library, pU6-sgRNA EF1Alpha-puro-T2A-BFP.

Table 1

KDR	Protospacer	5' forward	3' reverse complement
	GCTGCCAGACGGACTTTCTG	TTGGCTGCCAGACGGACTTTCTGGTTTAAGAGC	TTAGCTCTTAAACCAGAAAGTCCGTCTGGCAGCCAACAAG
	GCGCAAGTGATGCCCGGCGC	TTGGCGCAAGTGATGCCCGGCGCGTTTAAGAGC	TTAGCTCTTAAACGCGCCGGGCATCACTTGCGCCAACAAG
	GTCTAGAGAAGGAGGCGCGG	TTGGTCTAGAGAAGGAGGCGCGGGTTTAAGAGC	TTAGCTCTTAAACCCGCGCCTCCTTCTCTAGACCAACAAG
	GAGGCAGACAGGTCGGGTGA	TTGGAGGCAGACAGGTCGGGTGAGTTTAAGAGC	TTAGCTCTTAAACTCACCCGACCTGTCTGCCTCCAACAAG
	GGCGGCGCGCAAGTGATGCC	TTGGGCGGCGCGCAAGTGATGCCGTTTAAGAGC	TTAGCTCTTAAACGGCATCACTTGCGCGCCGCCCAACAAG
SRC			
	Gggcagacggacgcacggga	TTGGggcagacggacgcacgggaGTTTAAGAGC	TTAGCTCTTAAACTCCCGTGCGTCCGTCTGCCCCAACAAG
	Ggcgggacgtccagcgggac	TTGGgcgggacgtccagcgggacGTTTAAGAGC	TTAGCTCTTAAACGTCCCGCTGGACGTCCCGCCCAACAAG
	Gcggaccgcgggacgtccag	TTGGcggaccgcgggacgtccagGTTTAAGAGC	TTAGCTCTTAAACCTGGACGTCCCGCGGTCCGCCAACAAG
	Gcaccggcagacggacgcac	TTGGcaccggcagacggacgcacGTTTAAGAGC	TTAGCTCTTAAACGTGCGTCCGTCTGCCCGTGCCAACAAG
	Gggcgggcgggcgggctcac	TTGGggcgggcgggcgggctcacGTTTAAGAGC	TTAGCTCTTAAACGTGAGCCCGCCCGCCCGCCCCAACAAG
PAR1			
	GGTGCCCACGGGTAAGATCA	TTGGGTGCCCACGGGTAAGATCAGTTTAAGAGC	TTAGCTCTTAAACTGATCTTACCCGTGGGCACCCAACAAG
	GGGACCCTGATCTTACCCGT	TTGGGGACCCTGATCTTACCCGTGTTTAAGAGC	TTAGCTCTTAAACACGGGTAAGATCAGGGTCCCCAACAAG
	GTCAGGGTCCAAGCGACCCT	TTGGTCAGGGTCCAAGCGACCCTGTTTAAGAGC	TTAGCTCTTAAACAGGGTCGCTTGGACCCTGACCAACAAG
	GTGGCTTTCGGAGGAAACTG	TTGGTGGCTTTCGGAGGAAACTGGTTTAAGAGC	TTAGCTCTTAAACCAGTTTCCTCCGAAAGCCACCAACAAG
	GTCGGCGAGCGCTGTGTCTG	TTGGTCGGCGAGCGCTGTGTCTGGTTTAAGAGC	TTAGCTCTTAAACCAGACACAGCGCTCGCCGACCAACAAG
GNAQ			
	GACTGGAGCACAGATCCggg	TTGGACTGGAGCACAGATCCgggGTTTAAGAGC	TTAGCTCTTAAACCCCGGATCTGTGCTCCAGTCCAACAAG
	GGCTCCGCGCCTGGCAATCG	TTGGGCTCCGCGCCTGGCAATCGGTTTAAGAGC	TTAGCTCTTAAACCGATTGCCAGGCGCGGAGCCCAACAAG
	GGAGCACAGATCCgggaggg	TTGGGAGCACAGATCCgggagggGTTTAAGAGC	TTAGCTCTTAAACCCCTCCCGGATCTGTGCTCCCAACAAG
	GCTCCTTCCCCGGGAACAGG	TTGGCTCCTTCCCCGGGAACAGGGTTTAAGAGC	TTAGCTCTTAAACCCTGTTCCCGGGGAAGGAGCCAACAAG
	GCGCCAGGCGCACGGCGTAG	TTGGCGCCAGGCGCACGGCGTAGGTTTAAGAGC	TTAGCTCTTAAACCTACGCCGTGCGCCTGGCGCCAACAAG
negative control			
	GCTGCATGGGGCGCGAATCA	TTGGCTGCATGGGGCGCGAATCAGTTTAAGAGC	TTAGCTCTTAAACTGATTCGCGCCCCATGCAGCCAACAAG
	GTGCACCCGGCTAGGACCGG	TTGGTGCACCCGGCTAGGACCGGGTTTAAGAGC	TTAGCTCTTAAACCCGGTCCTAGCCGGGTGCACCAACAAG
	GTGTGCAACCTCCGCCGTTG	TTGGTGTGCAACCTCCGCCGTTGGTTTAAGAGC	TTAGCTCTTAAACCAACGGCGGAGGTTGCACACCAACAAG
	GCCCGAGCAGTGGCTCGCTA	TTGGCCCGAGCAGTGGCTCGCTAGTTTAAGAGC	TTAGCTCTTAAACTAGCGAGCCACTGCTCGGGCCAACAAG
	GGTCAGGTAGAGGGATTGAG	TTGGGTCAGGTAGAGGGATTGAGGTTTAAGAGC	TTAGCTCTTAAACCTCAATCCCTCTACCTGACCCAACAAG
Forward primer	gcacaaaaggaaactcaccct		

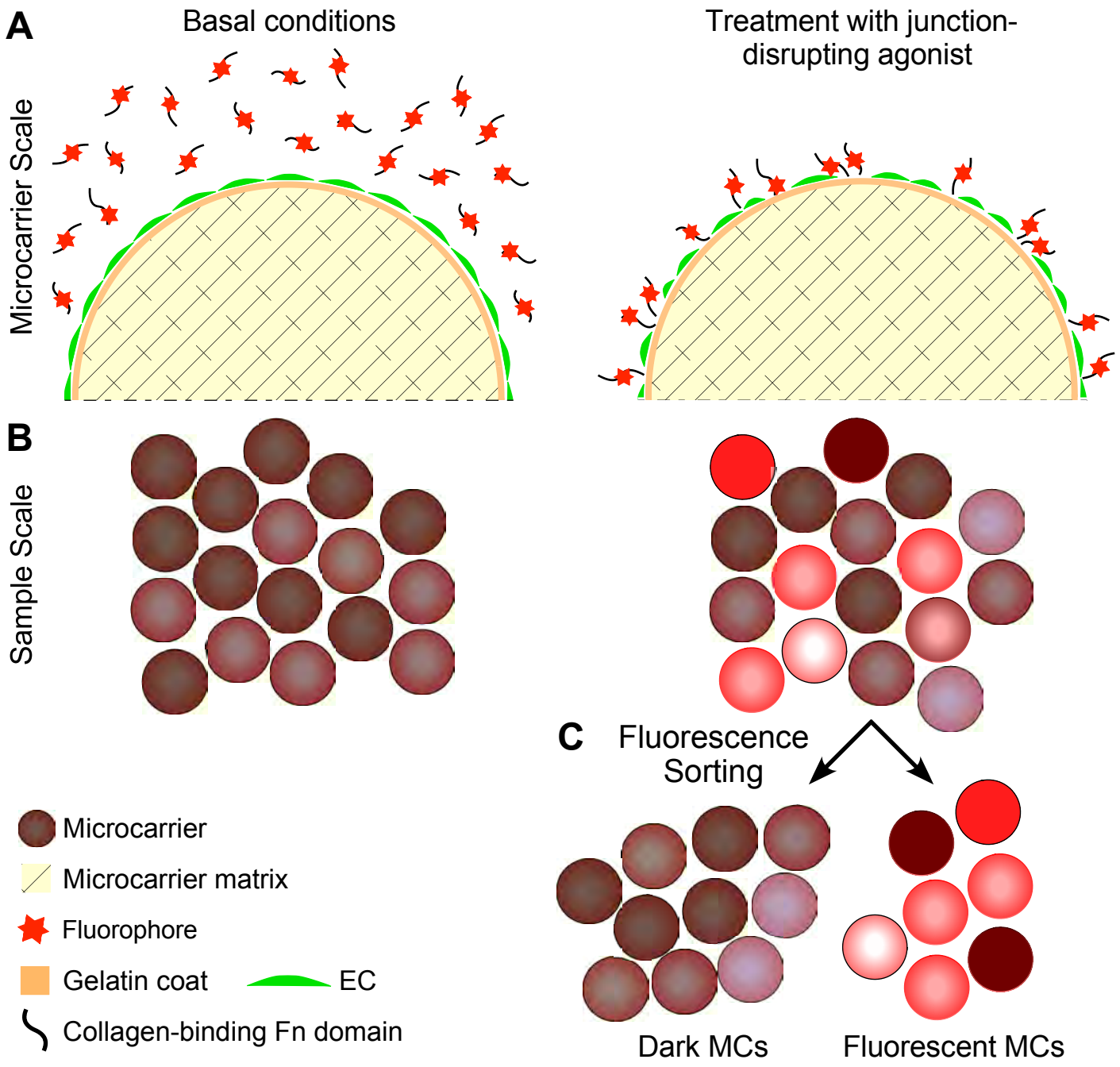
A
Basal conditions
Treatment with junction-disrupting agonist
Microcarrier Scale
B
Sample Scale
C
Fluorescence Sorting
Microcarrier
Microcarrier matrix
Fluorophore
Gelatin coat
EC
Collagen-binding Fn domain
Dark MCs
Fluorescent MCs

Figure 1

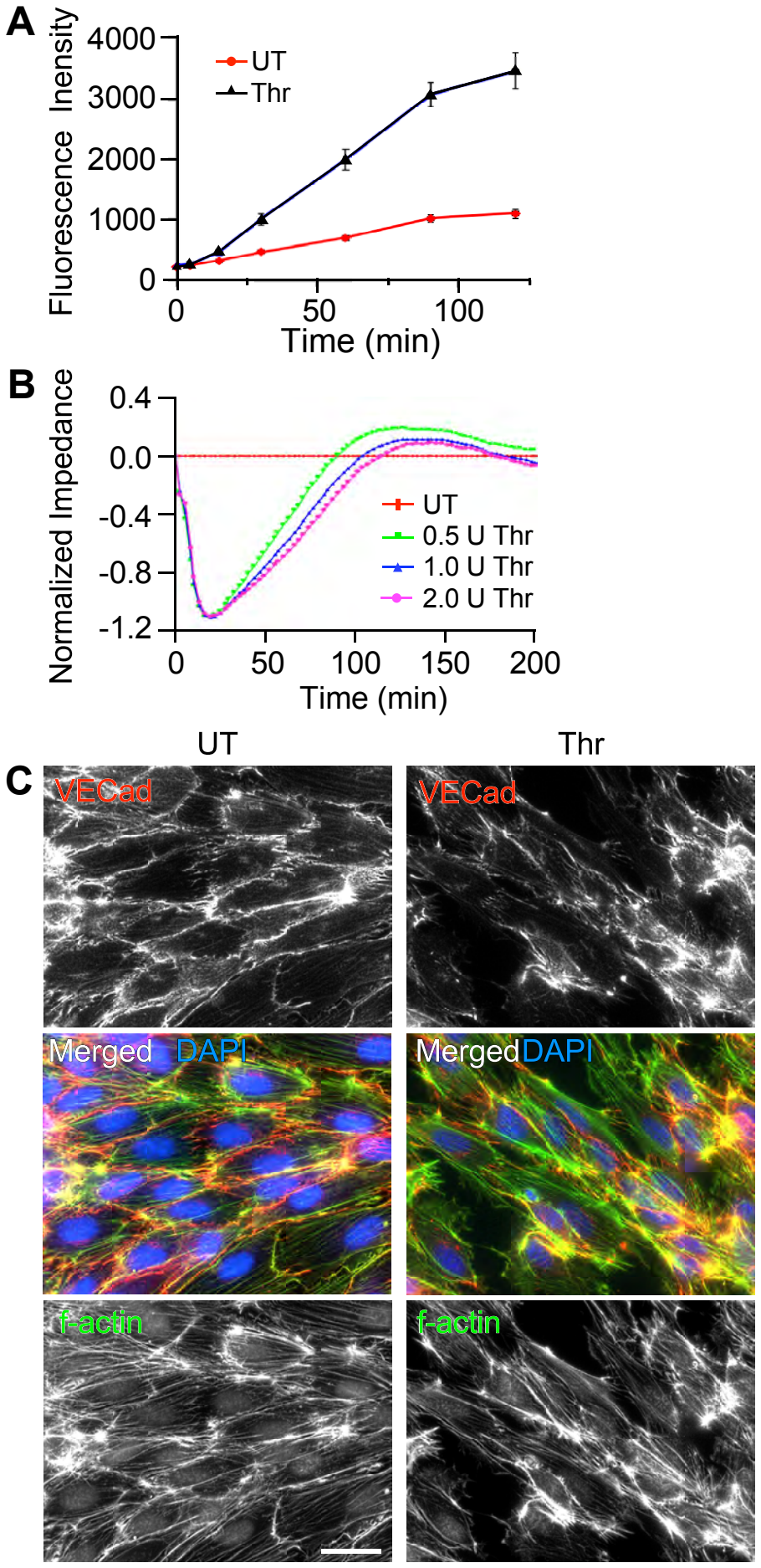
A
Fluorescence Inensity
4000
3000
2000
1000
0
UT
Thr
0
50
100
Time (min)
B
Normalized Impedance
0.4
0.0
-0.4
-0.8
-1.2
UT
0.5 U Thr
1.0 U Thr
2.0 U Thr
0
50
100
150
200
Time (min)
C
UT
Thr
VECad
VECad
Merged DAPI
MergedDAPI
f-actin
f-actin

Figure 2

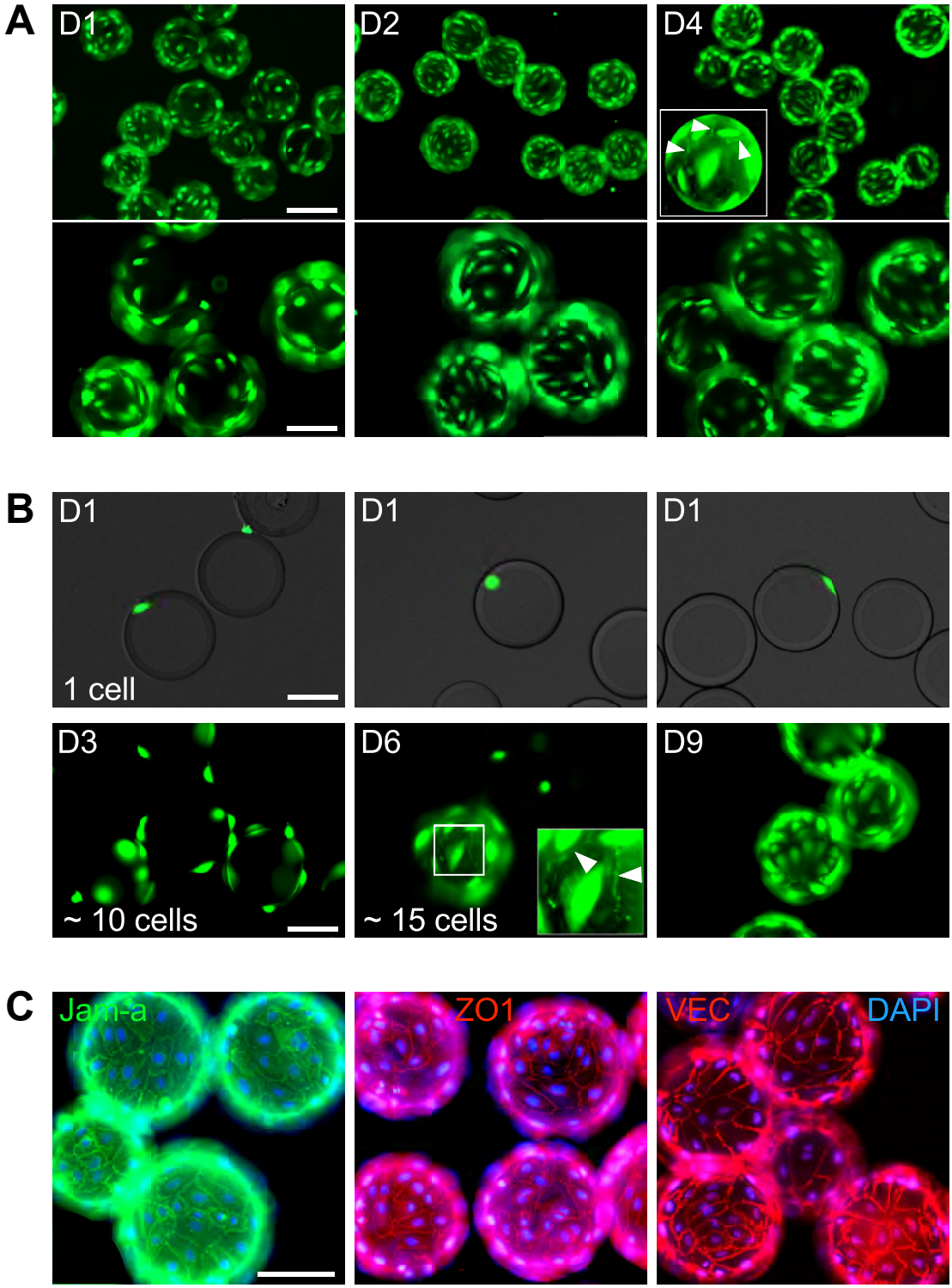
A
D1
D2
D4
B
D1
1 cell
D1
D1
D3
~ 10 cells
D6
~ 15 cells
D9
C
Jam-a
ZO1
VEC
DAPI

Figure 3

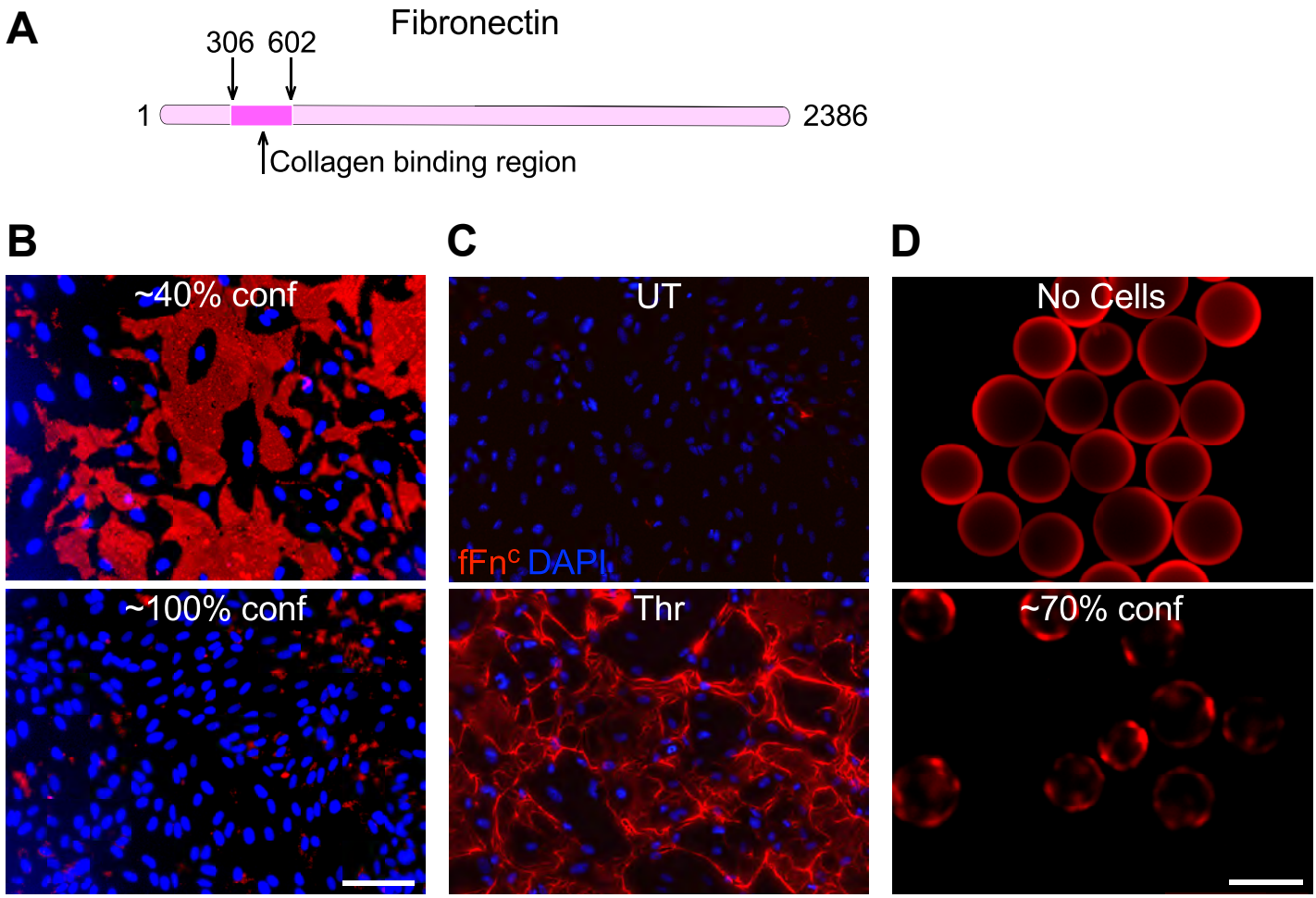
A
Fibronectin
306
602
1
2386
Collagen binding region
B
C
D
~40% conf
UT
No Cells
fFnc DAPI
~100% conf
Thr
~70% conf

Figure 4

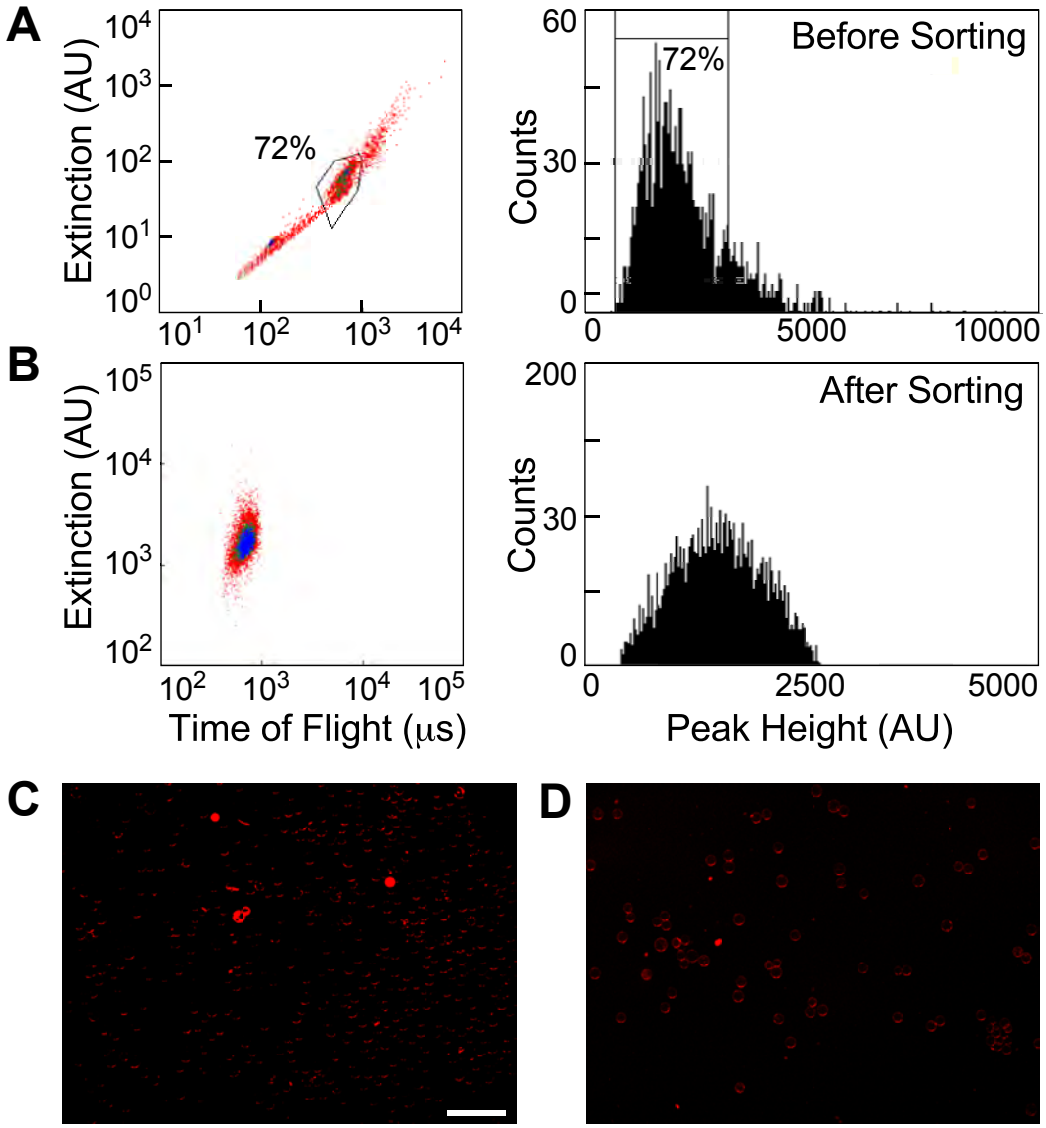
A
Extinction (AU)
72%
Before Sorting
Counts
72%
B
Extinction (AU)
After Sorting
Counts
Time of Flight (μs)
Peak Height (AU)
C
D

Figure 5

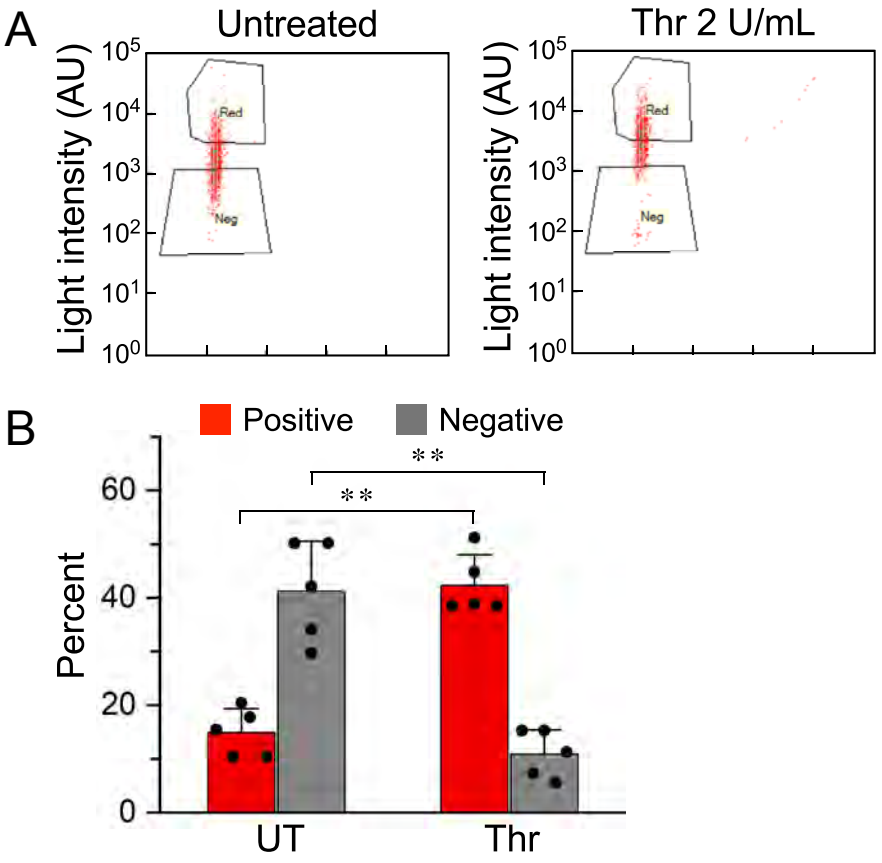
A
Untreated
Thr 2 U/mL
Light intensity (AU)
Red
Neg
B
Positive
Negative
Percent
UT
Thr
**
**

Figure 6

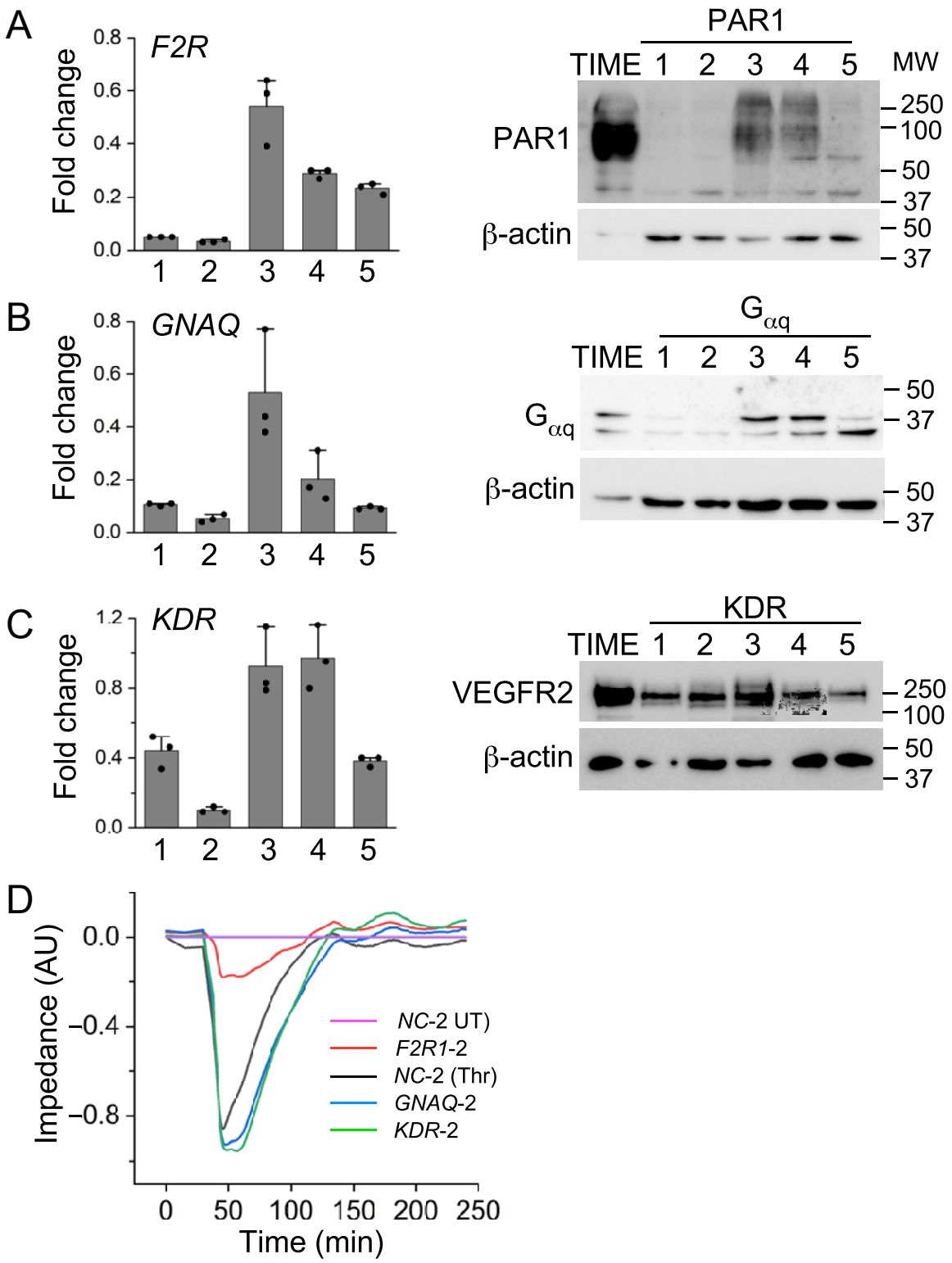
A
F2R
Fold change
0.8
0.6
0.4
0.2
0.0
1 2 3 4 5
PAR1
TIME 1 2 3 4 5
MW
PAR1
β-actin
250
100
50
37
50
37
B
GNAQ
Fold change
0.8
0.6
0.4
0.2
0.0
1 2 3 4 5
Gαq
TIME 1 2 3 4 5
Gαq
β-actin
50
37
50
37
C
KDR
Fold change
1.2
0.8
0.4
0.0
1 2 3 4 5
KDR
TIME 1 2 3 4 5
VEGFR2
β-actin
250
100
50
37
D
Impedance (AU)
0.0
−0.4
−0.8
0 50 100 150 200 250
Time (min)
NC-2 UT)
F2R1-2
NC-2 (Thr)
GNAQ-2
KDR-2

Figure 7

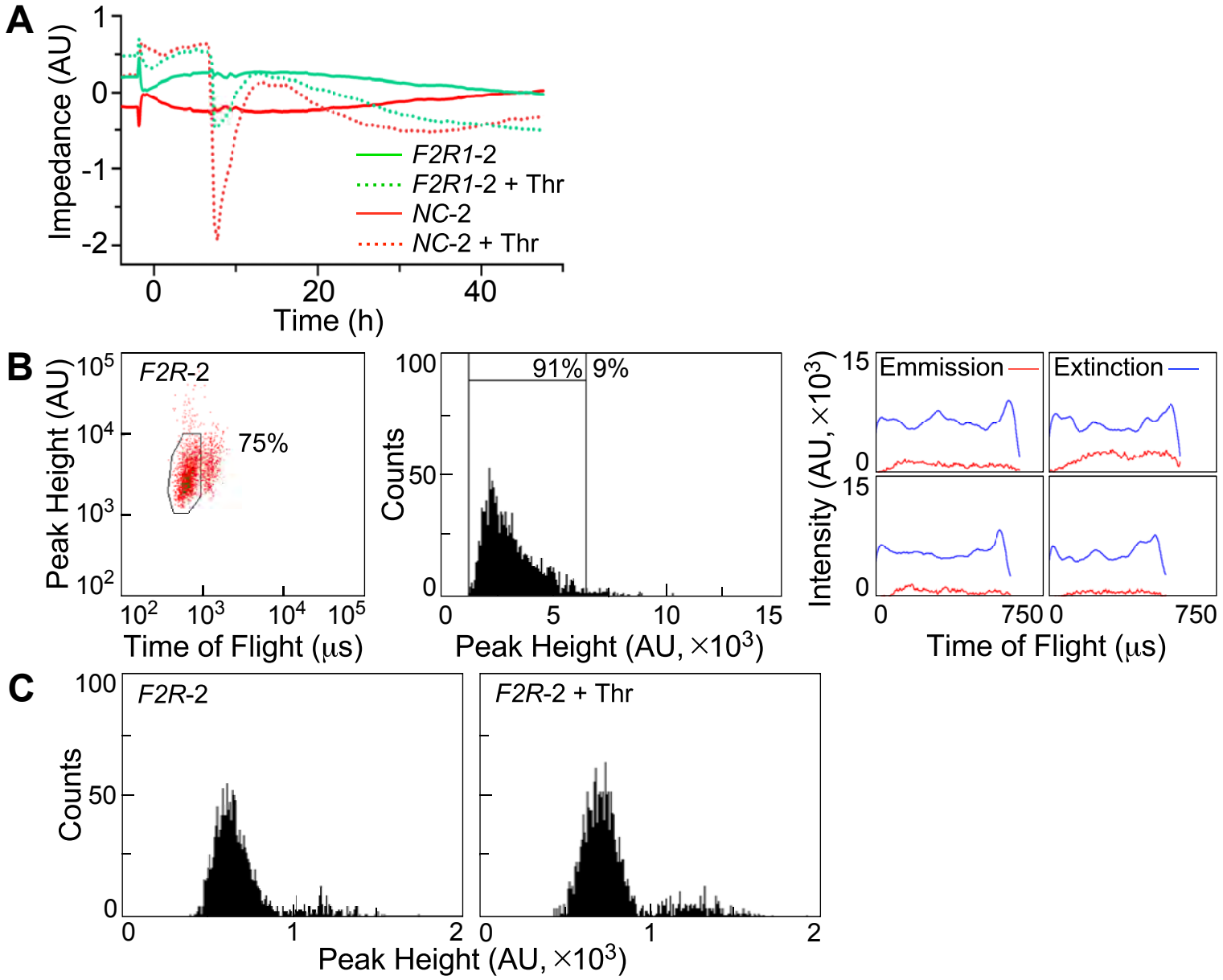
A
Impedance (AU)
1
0
-1
-2
0
20
40
Time (h)
F2R1-2
F2R1-2 + Thr
NC-2
NC-2 + Thr
B
Peak Height (AU)
F2R-2
75%
Time of Flight (μs)
Counts
91%
9%
Peak Height (AU, ×10³)
Intensity (AU, ×10³)
Emmission
Extinction
Time of Flight (μs)
C
F2R-2
F2R-2 + Thr
Counts
Peak Height (AU, ×10³)

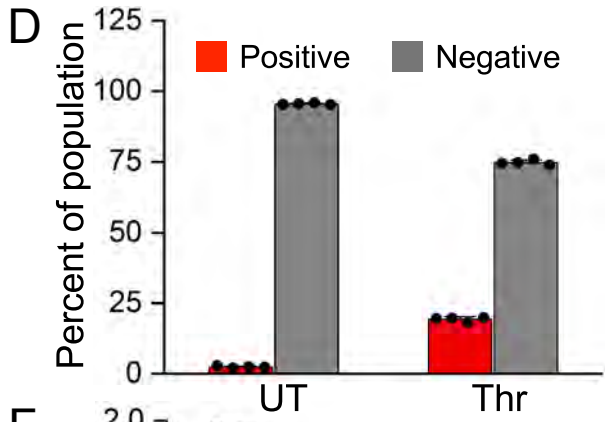
D
Percent of population
Positive
Negative
UT
Thr

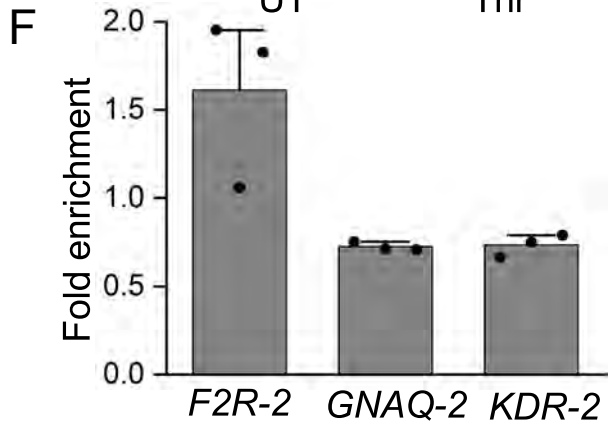
F
Fold enrichment
F2R-2
GNAQ-2
KDR-2

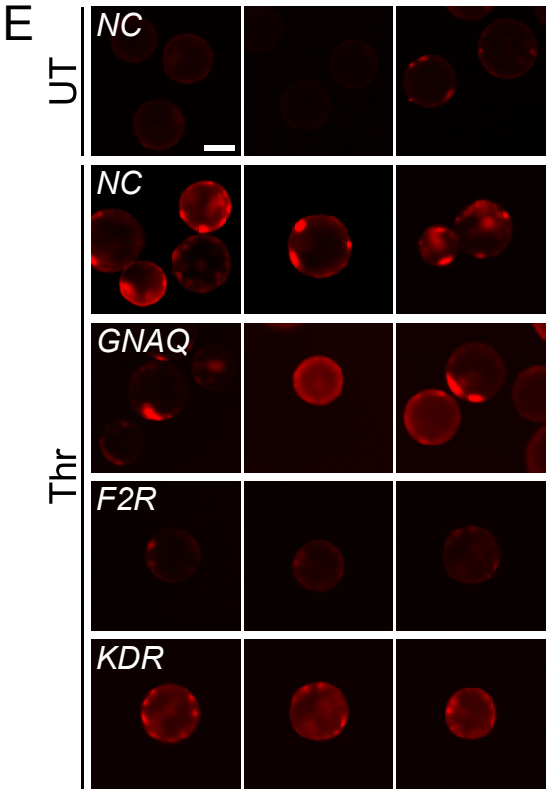
E
UT
Thr
NC
NC
GNAQ
F2R
KDR

Figure 8